Food Chemistry 181 (2015) 170–178

Contents lists available at ScienceDirect

Food Chemistry

journal homepage: www.elsevier.com/locate/foodchem

Stereoselective interaction of cinchona alkaloid isomers with bovine serum albumin

Yan Liu [a], Mingmao Chen [b], Longguang Jiang [a], Ling Song [a,*]

[a] The State Key Lab of Structural Chemistry, Fujian Institute of Research on the Structure of Matter, Chinese Academy of Sciences, Fuzhou, Fujian 350002, People's Republic of China
[b] Institute of Biomedical and Pharmaceutical Technology, Fuzhou University, Fuzhou, Fujian 350002, People's Republic of China

ARTICLE INFO

Article history:
Received 23 July 2014
Received in revised form 30 December 2014
Accepted 4 February 2015
Available online 14 February 2015

Keywords:
Cinchona alkaloid isomers
Bovine serum albumin
Stereoselective binding
Conformational change
Spectroscopic methods

ABSTRACT

The dependence of the interaction between bovine serum albumin (BSA) and two cinchona alkaloids, quinine (QN) and quinidine (QD), on the absolute configuration of these stereoisomers has been comprehensively studied. The FTIR spectra showed that QN and QD interacted with both C=O and C–N groups of BSA, resulting in changes to the secondary structure of the protein. Fluorescence quenching of BSA by the stereoisomers revealed lower efficiency for QD in quenching the Trp emission of BSA when compared to QN. Further analysis accurately described the different binding behaviors and recognition discrepancies of QN and QD towards BSA, which was reflected through binding affinities, driving forces, energy changes and conformational changes during the ligand–protein interactions. Synchronous fluorescence further proved that QD was farther from Trp and Tyr than that of QN. This work could provide basic data for clarifying the binding interaction, metabolism and distribution of cinchona alkaloid stereoisomers *in vivo*.

1. Introduction

Quinine (QN) and quinidine (QD), the chief quinoline alkaloids of various species of cinchona bark, are stereoisomers of each other and both contain two major fused-ring systems: the aromatic quinoline and the bicyclic quinuclidine (Scheme S1). In many parts of the world, quinine is a flavor component of tonic water and bitter lemon and is also widely used as an ingredient in other beverages (Horie et al., 2006; Worden, Frape, & Shephard, 1987). Due to its bitter taste, quinine tonics have been mixed with gin, by British colonials in India, to create a cocktail (Callaway & Tate, 1974; Ohira et al., 2013). As two stereoisomers of the family of quinoline alkaloids, the only conformational difference between QN and QD is the opposite configurations of two chiral centers (Karle, Karle, Gerena, & Milhous, 1992). Due to the conformational discrepancy, these two stereoisomers possess different physiological activities in the human body. QN is antimalarial, analgesic and anti-inflammatory, while QD is often used as an antiarrhythmic drug in treating a rare form of congenital myasthenia (Kellogg et al., 1989; Zaugg & Thormann, 2001). The different physiological behavior between QN and QD is probably influenced by the unequally binding behavior of the stereoisomers towards transport protein, target protein and other biomolecules in human body, which is induced by the different spatial conformations of QN and QD.

The binding of exogenous compounds to plasma proteins in biological systems is of interest because of their potential applications in cosmetics, foods, pharmaceuticals and physiological systems (Lazaro, Lowe, Briand, & Faller, 2008; Zhang & Ma, 2013). As an intrinsic property of many biological systems, chirality plays a major role in the binding activities between chiral ligands and carrier proteins. The potentially different binding behaviors of the stereoisomers to plasma proteins can cause the difference in their biological properties (Izake, 2007; Lu, 2007). Thus, studies on the chiral discrimination of stereoisomers by binding to biomacromolecular hosts are essential for understanding the biodistribution, metabolism, elimination and physiological effects of chiral compounds in human body.

In this respect, serum albumins have been intensively studied with respect to their roles in the transport of physiological ligands. Serum albumins are the major soluble plasma proteins of the blood circulatory system *in vivo* (Carter & Ho, 1994; Peters, 1985), which are considered to possess efficient stereoselectivities among plasma proteins and exhibit chiral recognition abilities upon complexation with a variety of chiral compounds (Kumar, Buranaprapuk, & Sze, 2001; Otagiri & Chuang, 2006). Bovine serum albumin (BSA) consists of 583 amino acid residues and is composed of three homologous domains (I, II and III) and each domain includes two subdomains (A and B). It contains 17 disulfide bridges that divide the protein into 9 loops. It has two tryptophan residues as intrinsic fluorophores: Trp-134, located on the surface of subdomain IB, and Trp-212, located in the hydrophobic binding pocket of

* Corresponding author. Tel.: +86 591 83720913; fax: +86 591 83722697.
E-mail address: songling@fjirsm.ac.cn (L. Song).

http://dx.doi.org/10.1016/j.foodchem.2015.02.040
0308-8146/

subdomain IIA (Carter & Ho, 1994; Liu, Chen, Luo, Lin, & Song, 2013; Peters, 1985). The intrinsic fluorescence of Trp facilitates the investigations of binding behaviors between the endogenous or exogenous ligands and BSA. BSA is one of the most extensively studied plasma proteins not only because of its structural homology with HSA, but also due to its good availability, low cost and medical importance.

The binding affinity between QN/QD and serum albumin is an important factor to understand the physiological properties of cinchona alkaloid stereoisomers as it strongly influences their distribution and determines the free fraction that is available for subsequent interactions with targeted receptors. However, there are only a few detailed studies regarding the protein binding properties of chiral cinchona alkaloids at the molecular level. In this work, the stereoselective binding interactions for the cinchona alkaloid isomers towards BSA were systematically investigated under physiological conditions by spectroscopic methods including FTIR, fluorescence spectroscopy, UV–Vis absorption spectra and circular dichroism analysis. These methods provided general information for the ligand–protein complex, such as quenching rate constants, binding modes, binding constant and thermodynamic parameters. Structural information regarding the stereoisomer binding mode and the effect of QN/QD–BSA complexation on the protein stability and secondary structure was clarified here. The present results contribute to elucidate the mechanisms of transporting and targeting of chiral cinchona alkaloids by carrier proteins and to further understand the correlations between the spatial conformation and physiological activities of stereoisomeric ligands *in vivo*.

2. Materials and methods

2.1. Reagents

Bovine serum albumin (BSA) was purchased from Sinopharm Chemical Reagent Beijing Co., Ltd. (Beijing, China). Quinine (QN) and quinidine (QD) were purchased from Alfa Aesar Reagent Company. All other reagents used were of analytical grade. Double-distilled water with a resistivity of 18.2 MΩ (Milli-Q water, Millipore, USA) at room temperature (25 °C) was used throughout experiments. BSA was dissolved in 0.05 M phosphate buffered saline solution (PBS) to form a solution with required concentration (pH 7.4), and then preserved at 4 °C for later use.

2.2. Apparatus

Fourier transform infrared spectra (FTIR) were recorded on a Spectrum One FTIR spectrometer (Perkin-Elmer corporate, USA). Fluorescence data were obtained on a Cary Eclipse Spectrofluorimeter (Varian corporate, USA) equipped with 1.0 cm quartz cells. Absorption spectra were recorded on a Lambda-35 spectrophotometer (PerkinElmer corporate, USA) equipped with 1.0 cm quartz cells at room temperature. Circular dichroism (CD) spectra were measured on a MOS-450/AF-CD Spectropolarimeter (Bio-Logic corporate, France) with a 1 mm quartz cell at room temperature under constant nitrogen flush. All pH measurements were conducted with a PHS-3C acidity meter.

2.3. Methods

Samples for the infrared measurements were prepared essentially as described above in a D_2O buffer containing 100 mM NaCl, 100 mM phosphate with pD = 7.4. The sample solution was added dropwise to the protein solution with constant stirring at 4 °C to ensure the formation of a homogeneous solution at the target concentrations. Then, an aliquot of the sample (approximately 40 μl) was placed between two CaF_2 windows using 50 μm Teflon spacers. Each spectrum was obtained by collecting 256 interferograms with a nominal resolution of 2 cm^{-1}. Derivation and Fourier self-deconvolution were applied in order to resolve the component bands of the amide I region of the spectrum.

For the fluorescence analysis of protein titrated by ligand, QN/QD solution was added into the BSA solutions in sequence. Both QN/QD and BSA concentrations were calculated by weight for consistency. The systems were excited at 280 nm and the emission wavelength was adjusted from 300 to 500 nm with a scanning speed of 600 nm min^{-1}. The excitation and emission slit widths were both set at 5.0 nm.

For the fluorescence analysis of ligand titrated by protein, the solution of QN/QD in 0.05 M phosphate buffer (pH 7.4) was titrated with BSA. Each resultant solution through the titration was allowed to stand for 10 min, and then its fluorescence emission spectrum was recorded between 350–525 nm with a scanning speed of 600 nm min^{-1}. The excitation and emission slits were set to 10.0 nm and 5.0 nm, respectively. All the experiments were conducted in triplicate.

For UV–Vis absorption spectra, the sample solution with fixed concentration was added to a 10 ml volumetric flask, and then made up to volume with PBS solution. The equilibrated solution was poured into quartz cells (4 cm × 1 cm × 1 cm) and scanned in the ultraviolet range (190–350 nm) using PBS solutions (pH = 7.40) as references.

Circular dichroism (CD) spectra were measured on a MOS-450/AF-CD spectropolarimeter at room temperature under constant nitrogen flush. The path length and volume of quartz cells were 0.1 cm and 400 μl, respectively. The scanning speed was set at 100 nm min^{-1}. Each spectrum was measured 3 times in succession and the PBS buffer solutions treated under the same conditions were taken as blank.

Synchronous fluorescence spectra of aqueous solutions prepared as described above were measured on the Cary Eclipse fluorescence spectrophotometer. The initial excitation wavelength (λ_{ex}) was set at 280 nm. The excitation and emission slit widths were both set at 5 nm. The D-value ($\Delta\lambda$) between the excitation and emission wavelengths was set at 15 or 60 nm, at which the spectrum only showed the spectroscopic behavior of Tyr and Trp residues of BSA, respectively.

Molecular theoretical calculations were carried out using ICM (v3.4–8) software. The native structure of BSA (PDB ID 3V03) was taken from Protein Data Bank with a crystalline resolution at 2.70 Å. All water molecules were removed and local search was used to search for the optimum binding site of small molecules to the protein. A grid size of 90 × 90 × 90 points with a grid spacing of 0.4 Å was applied. The docking conformation with the lowest binding free energy was further processed by Pymol software.

3. Results and discussion

3.1. FTIR study on secondary structural changes of BSA

The infrared spectra of proteins are mainly comprised of amide I (1600–1700 cm^{-1}) and amide II (1500–1600 cm^{-1}), which are caused by the carbonyl stretching vibrations of the peptide backbone (amide I band) and the combination of N–H in-plane bending and C–N stretching vibrations of peptide groups (amide II band) (Charbonneau & Tajmir-Riahi, 2010). Generally, the amide I band is more sensitive to changes in protein secondary structure than the amide II band. The overall shape of the amide I band is determined by the various secondary structure components, such as α-helix (1650–1660 cm^{-1}), β-sheet (1610–1640 cm^{-1}), turn

structure (1660–1680 cm^{-1}), β-antiparallel (1680–1692 cm^{-1}) and random coil (1641–1648 cm^{-1}) (Mantsch & Chapman, 1996; Vaden et al., 2007). Conformational changes of proteins usually happen during ligand–protein complexation process. The infrared self deconvolution with second derivative resolution enhancement and curve-fitting procedures could be applied to determine the secondary structure of BSA. Herein, the interaction between QN/QD and BSA was characterized by FTIR spectroscopy. A quantitative analysis of the protein secondary structure for the free BSA and QN/QD–BSA complex in hydrated films were carried out.

As shown in Fig. 1 and Table S1, an intense band in the amide I region centered at 1650 cm^{-1} could be observed in the original FTIR spectra of free BSA without QN/QD, indicating that BSA is in an α-helix rich conformation. According to Fig. 1 and Table S1, the free BSA had 55.68% α-helix, 19.46% β-sheet, 9.58% turn structure, 2.94% β-antiparallel and 12.34% random coil. At low ligand concentration (<20 μM), there were no apparent peak shifts for BSA and Q–BSA complex. However, an relatively significant decrease of α-helix from 55.68% (free BSA) to 43.28% (10 μM QN) and 45.07% (10 μM QD), 40.63% (20 μM QN) and 42.86% (20 μM QD) with an increase in turn structure from 9.58% (free BSA) to 20.44% (10 μM QN) and 18.90% (10 μM QD), 21.42% (20 μM QN) and 22.32% (20 μM QD) was observed. It was also noted that some remarkable changes were observed for the random coil (from 12.34% without ligand to 19.95% for 10 μM QN and 21.52% for 10 μM QD), β-sheet structure (from 19.46% without ligand to 15.07% for 10 μM QN and 12.52% for 10 μM QD) and β-antiparallel (from 2.94% without ligand to 1.26% for 10 μM QN and 1.99% for 10 μM QD). In the presence of QN/QD with high concentration (100 μM), the band in the QN/QD–BSA complex system showed obvious changes in both shape and peak position, which were due to the relatively stronger binding of QN/QD towards the C=O, C–N and N–H groups of protein, which induced the rearrangement of the polypeptide carbonyl hydrogen bonding pattern (Belatik, Hotchandani, Carpentier, & Tajmir-Riahi, 2012). The proportion of α-helix significantly reduced to 37.68% (QN–BSA complex) and 39.17% (QD–BSA complex) accompanied by a major increase in turn (23.96% for QN, 25.56% for QD) and random coil (20.15% for QN, 24.55% for QD). Besides, the shifting of the protein amide A band in infrared spectra from 3291 cm^{-1} (N–H stretching mode) in the free BSA to 3286 cm^{-1} (QN–BSA system) and 3288 cm^{-1} (QD–BSA system) is additional evidence to support the notion that QN/QD binds with C–N and N–H groups upon ligand–protein complexation (spectra not shown).

The protein CH_2 antisymmetric and symmetric stretching vibrations, in the region of 3000–2800 cm^{-1}, were examined to detect the presence of hydrophobic contact in the QN/QD–BSA complexes (Fig. S1). The CH_2 bands of the free BSA at 2960, 2935 and 2875 cm^{-1} shifted to 2959, 2934 and 2873 cm^{-1} (QN–BSA) and 2961, 2937 and 2874 cm^{-1} (QD–BSA) upon ligand–protein interactions. The subtle shifting of the protein antisymmetric and symmetric CH_2 stretching vibrations suggested the hydrophobic interactions might make a slight contribution to the QN/QD–BSA interaction. According to the FTIR analysis results, it could be speculated that some α-helix might be converted into random coil and turn structure when BSA was conjugated with QN/QD. The major reduction of α-helix and other secondary structural changes might suggest the destruction of the hydrogen bond of BSA and a certain degree of protein unfolding in the presence of cinchona alkaloid isomers. The different structural changes of BSA observed in FTIR spectra indicated the stereoselective-dependent discrepancies in the binding mode between QN and QD towards protein.

3.2. Fluorescence spectra

3.2.1. Eliminate the inner filter effect

Since the inner filter effect (IFE) may affect fluorescence measurements due to the formation of ligand–protein complex, we took advantage of some effective methods to correct the fluorescence of the complex and reduce the IFE (Lakowicz, 2006). Firstly,

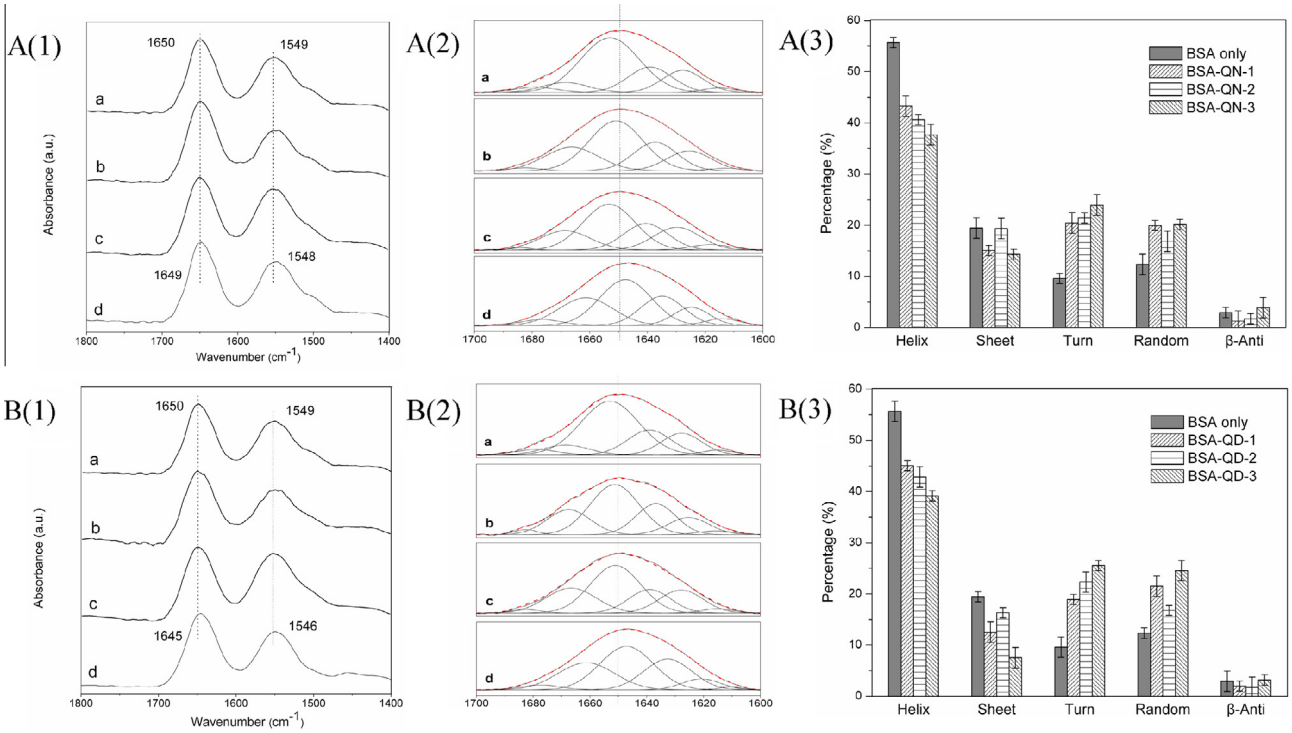

Fig. 1. FTIR analysis for QN–BSA system (A) and QD–BSA system (B); FTIR adsorption spectra in the region of 1800–1400 cm^{-1} (1); the curve-fitted spectra of the amide I band for free BSA and Q–BSA complex (2); fraction of the secondary structure of proteins as determined by quantitative curve-fitting analysis (3). The value was obtained from three experiments, and the error bars indicate standard deviations from the mean. Conditions: [BSA] = 1.0×10^{-5} mol l^{-1}; [Q] (a–d), 0, 1, 2 and 10×10^{-5} mol l^{-1}.

each fluorescence spectrum of BSA in the presence of different concentrations of QN/QD was corrected for any possible IFE using the following equation (Eq. (1)):

$$F_{cor} = F_{obs} 10^{\frac{A_{ex} \cdot d_{ex}}{2} + \frac{A_{em} \cdot d_{em}}{2}} \quad (1)$$

where F_{cor} is the corrected fluorescence intensity obtained in the absence of inner-filter effect; F_{obs} is the measured fluorescence; A_{ex} and A_{em} are the sum of the absorbances of protein and ligand at the excitation and emission wavelengths, respectively; d_{ex} and d_{em} are the cuvette pathlength in the excitation and emission direction (in cm), respectively. Furthermore, in order to reduce as much as possible the inner filter effect caused by the absorption of both excitation radiation and emission radiation, we controlled the BSA concentration to be 2.0×10^{-6} mol l^{-1}, and the maximum concentration of Q to be 5.25×10^{-5} mol l^{-1}. Thus, any possible contribution of inner filter effect due to attenuation of the incident light by the quencher could be negligible. In addition, fluorescence backgrounds were also corrected for blank buffer solutions in each measurement.

3.2.2. Effect of cinchona alkaloid isomers on the fluorescence spectra of BSA

The characteristic of the intrinsic fluorescence of BSA is very sensitive to its microenvironment, so changes in the intrinsic fluorescence of BSA can provide valuable information about its structure and dynamics (Martin, Rodriguez, Maestre, & Moya, 2013). To understand the effect of cinchona alkaloid stereoisomers complexation on the protein, the fluorescence of the protein was further monitored. The emission spectra of BSA in the presence of different concentrations of cinchona alkaloid isomers were shown in Fig. 2. It was obvious that BSA had a strong fluorescence emission peaked at 348 nm after being excited with a wavelength of 280 nm. The presence of increasing amounts of QN/QD led to a decrease in the protein fluorescence, indicating the binding of QN/QD to the protein. Meanwhile, a red shift of the emission peak for both QN/QD–BSA systems also occurred, which provided evidence that the fluorescence chromophores of BSA were gradually exposed to solvent owing to protein unfolding and then being placed in a more hydrophilic environment after the addition of QN/QD (Lanone, Andujar, Kermanizadeh, & Boczkowski, 2013; Zhao & Liu, 2012). The fluorescence results also suggested that the microenvironment around the Trp and Tyr residues of BSA had been changed, causing an unfolded protein structure during the interaction with two cinchona alkaloid isomers. Besides, QN was likely to have a greater impact on the local dielectric environment of BSA than that of QD. The extinction of BSA tryptophans by QN decreased more rapidly than those caused by QD. It was worth noting that, at the concentration of 5.2×10^{5} mol l^{-1}, QN was found to lead to 25.2% quenching, while QD quenched 17.9% of BSA fluorescence. From the slopes of the curves, it could be preliminary concluded that the binding affinity of QN to BSA was stronger than that of QD.

3.2.3. The BSA fluorescence quenching mechanism

Fluorescence quenching is usually classified into two processes: static and dynamic quenchings. In order to find out the binding mechanism between BSA and QN/QD, the Stern–Volmer equation

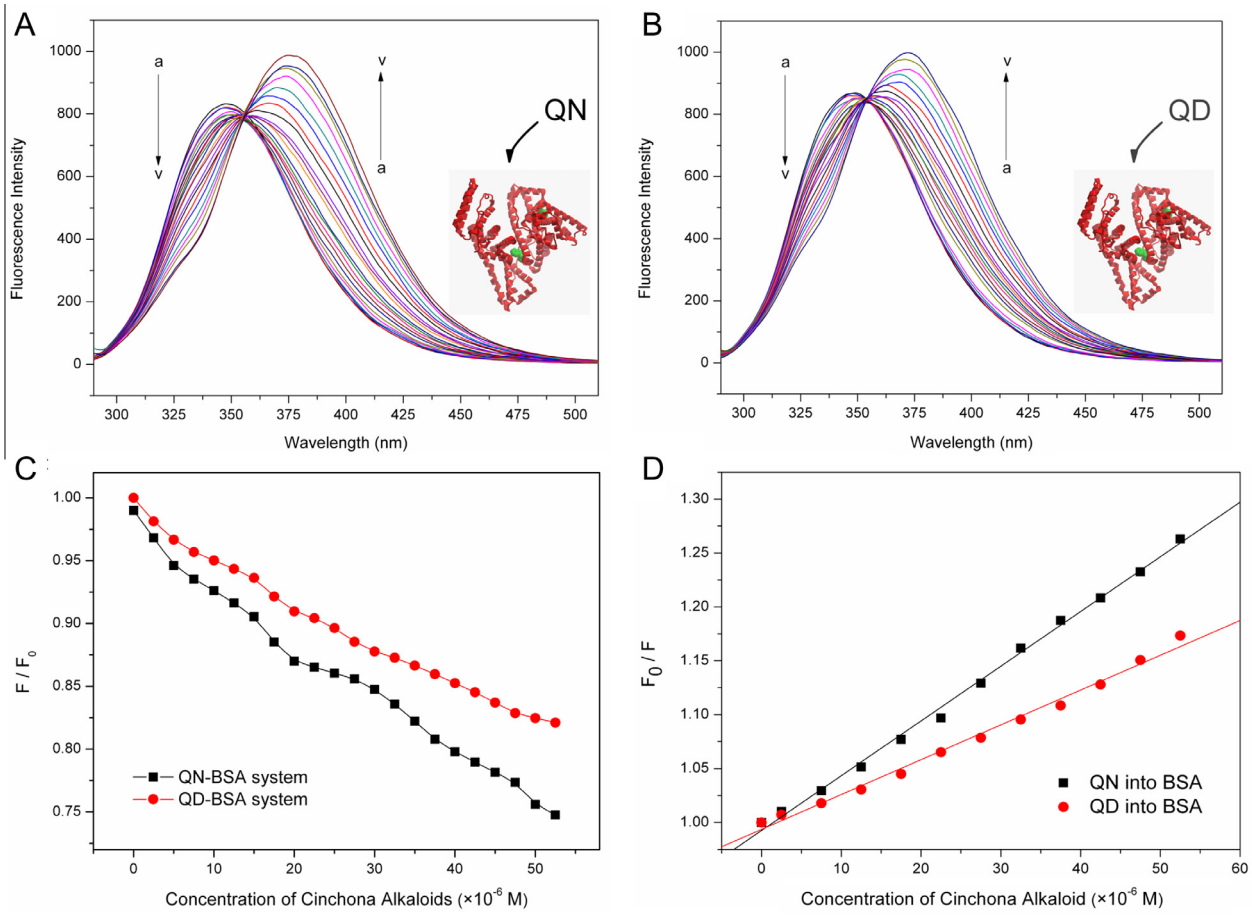

Fig. 2. (A) Effect of QN on BSA fluorescence at 293 K; (B) effect of QD on BSA fluorescence at 293 K; (C) The dependence of the fluorescence intensities of BSA by QN/QD at corresponding concentrations; (D) Stern–Volmer plots for the fluorescence quenching of BSA by the addition of QN/QD. Conditions: [BSA] = 2.0×10^{-6} mol l^{-1}; [Q] (a–v), 0–5.25×10^{-5} mol l^{-1} at increment of 0.25×10^{-6} mol l^{-1}.

has been employed here (Eq. (2)) (Chi & Liu, 2011; Kuhnemuth & Seidel, 2001):

$$\frac{F_0}{F} = 1 + K_q \tau_0 [Q] = 1 + K_{SV}[Q] \quad (2)$$

where F_0 and F are the steady-state fluorescence intensities without and with quencher QN/QD, respectively; K_q is the quenching rate constant; τ_0 represents the biomolecular average fluorescence lifetime; K_{SV} is the Stern–Volmer quenching constant and [Q] is the concentration of the quencher. τ_0 is the average lifetime of the molecule in the excited state without any quencher. Herein, the possible quenching mechanism of QN/QD–BSA binding can be analyzed with the fluorescence quenching spectra of BSA and the Stern–Volmer plots for QN/QD–BSA system at different temperatures. Static quenching is caused by ground-state complex formation among fluorophores. Therefore, increasing temperature will decrease the quenching constant K_{SV} due to the declined stability of ligand–protein complex in a static quenching system. In contrast, dynamic quenching results from collision between a fluorophore and a quencher (Lakowicz, 1999). Thus, the value of K_{SV} will increase with increasing temperature in a dynamic quenching system.

The plot of F_0/F versus [Q] was linear, which was indicative of one type of quenching in the QN/QD–BSA system. The values of K_{SV} derived from these plots were $5.16 \times 10^3\ l\ mol^{-1}$ and $3.07 \times 10^3\ l\ mol^{-1}$ for the binding of QN and QD forms at 298 K (Table S2). K_q, values calculated from the ratio of K_{SV}, were $8.51 \times 10^{11}\ l\ mol^{-1}\ S^{-1}$ and $5.06 \times 10^{11}\ l\ mol^{-1}\ S^{-1}$ for QN and QD, respectively. These values are in close agreement with the K_{SV} values obtained from the fluorescence quenching of the protein by QN/QD (*vide supra*). For dynamic quenching, the maximum value of the scattering collision quenching constant is $2 \times 10^{10}\ M^{-1}\ s^{-1}$ (Lakowicz, 1999; Vaughan & Weber, 1970). Since the values of the biomolecular quenching in QN/QD–BSA system are much higher than this value, it can be assumed that the complex formation between the cinchona alkaloid isomers and the protein is by a static mechanism. Moreover, the static quenching mechanism was further confirmed from the temperature dependence of the quenching. It was noted that the K_{SV} values decreased with increasing temperatures, indicating the weakening of the QN/QD–BSA complex. This result confirmed that the cinchona alkaloid isomer induced fluorescence quenching of BSA was caused by the ground state complex formation rather than by dynamic collision.

3.2.4. Binding constants and number of binding sites

The static mechanism is principally responsible for the observed fluorescence quenching when cinchona alkaloid isomers binds to BSA as discussed above. In order to investigate the equilibrium between free and bound molecules and rationalize our experimental data on the QN/QD–BSA systems, the following equation was employed (Eq. (3)):

$$\log \frac{(F_0 - F)}{F} = \log K_a + n \log[Q] \quad (3)$$

where F_0, F and [Q] are the same as in Eq. (2). According to Eq. (3), the values of K_a and n at physiological pH (7.4) could be calculated. The results for the two cinchona alkaloid isomers at different temperatures (293, 298 and 303 K) were given in Fig. S2 and Table 1. The number of binding sites n approximately equaled 1, indicating that there was only one binding site in BSA for QN/QD during their binding process. The binding constant (K_a) decreased with increasing temperature, indicating destabilization of the QN/QD–BSA complex with the rising temperature. Compared to QN, QD exhibited less affinity to BSA, which might be responsible for its lower quenching effectiveness. In general, the high affinities of binding constants in ligand–protein complexes locate in the range of 10^6–$10^8\ l\ mol^{-1}$. However, the obtained binding constants of QN/QD–BSA systems were relatively low (10^3–$10^4\ l\ mol^{-1}$), which indicated a medium level of binding interaction between QN/QD and BSA.

3.2.5. Effect of BSA on the fluorescence spectra of cinchona alkaloid isomers

Cinchona alkaloids are highly fluorescent in aqueous solution and are widely used as a standard for fluorescence quantum yield measurements (Lakowicz, 1999). Herein, the formation of specific ligand–protein complexes was further confirmed by monitoring the fluorescence changes of QN/QD upon binding to BSA. As shown in Fig. 3, QN and QD had emission maxima at 388 and 385 nm, respectively. An increase in the concentration of BSA resulted in the fluorescence quenching of both cinchona alkaloid isomers. The changes in the emission intensity of QN and QD at all protein concentrations seem similar whereas a certain difference between the effects of addition of macromolecules on the emission spectra of QN and QD could be observed at higher concentrations of BSA. The observed changes in the fluorescence spectra of the QN/QD can be rationalized in terms of binding of the probe compounds with the proteins, leading to a less polar microenvironment around the fluorophore. Binding of the isomers to the binding pocket of the protein might induce the organic group of QN/QD rotate or vibrate. The structural changes can be considered as another reason for decreased emission intensity of cinchona alkaloids. A blue shift in the fluorescence maximum also suggested a reduction in the polarity of the microenvironment. The binding interactions were further quantified in terms of Stern–Volmer quenching plots. According to Fig. 3C, the K_{SV} values obtained from this experiment for QN and QD binding to BSA were 10.73 and $8.83 \times 10^3\ l\ mol^{-1}$ at 298 K, respectively, indicating the binding capacity of QN towards BSA was larger than that of QD.

3.3. Thermodynamic parameters

The binding forces between ligand and protein include hydrogen bonds, van der Waals interactions, electrostatic forces and hydrophobic interaction forces, which can be determined by the thermodynamic parameters. The enthalpy change (ΔH) and the entropy change (ΔS) for the interaction between QN/QD and BSA were calculated according to the van't Hoff equation (Eq. (4)) (Pace, Shirley, McNutt, & Gajiwala, 1996; Ross & Subramanian, 1981):

$$\ln K_a = -\frac{\Delta H}{RT} + \frac{\Delta S}{R} \quad (4)$$

Table 1
Binding constants and relative thermodynamic parameters of QN/QD towards BSA at different temperatures.

Sample	T (K)	K_α ($\times 10^4\ l\ mol^{-1}$)	n	ΔG (kJ mol^{-1})	ΔH (kJ mol^{-1})	ΔS (J mol^{-1} K^{-1})
QN	283	1.185	1.222	−22.06	−17.54	16.07
	298	0.846	1.088	−22.39		
	313	0.579	0.962	−22.54		
QD	283	0.717	1.198	−20.88	−18.88	7.09
	298	0.485	1.127	−21.02		
	313	0.332	1.006	−21.09		

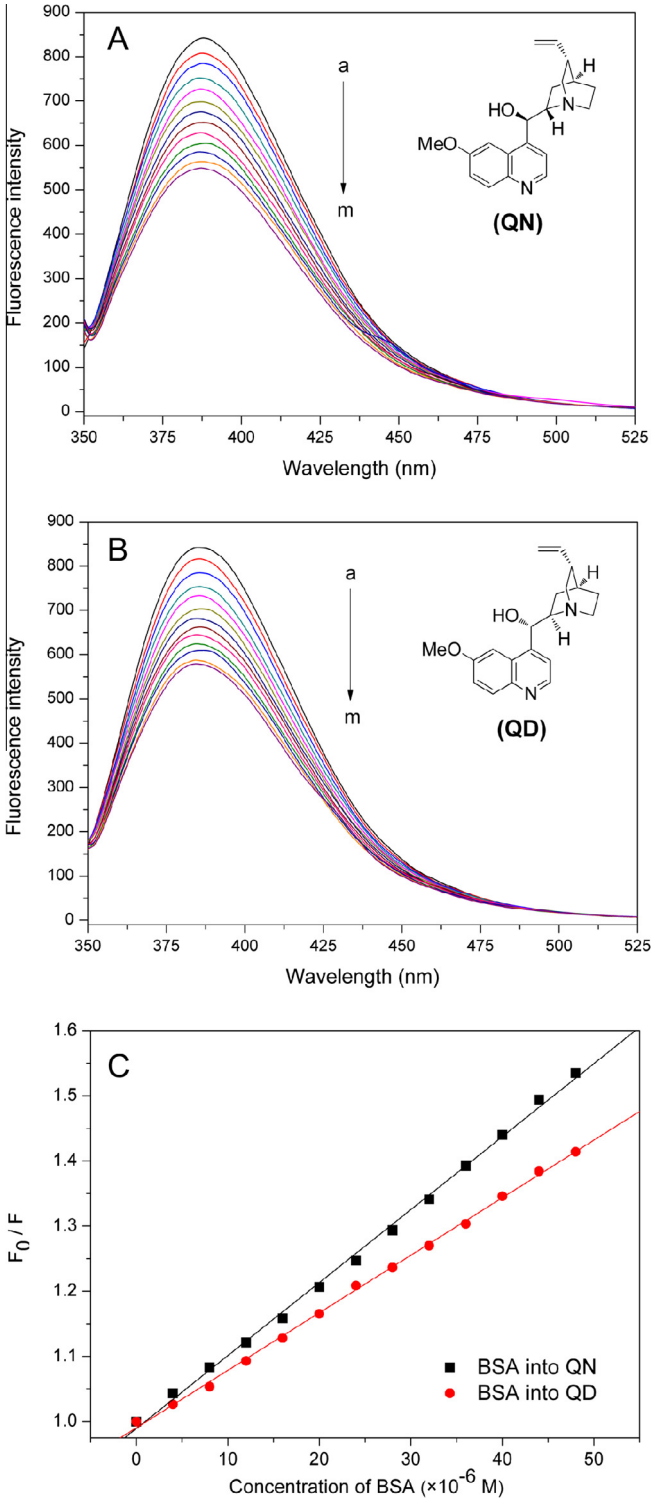

Fig. 3. (A) Effect of BSA on QN fluorescence at 293 K; (B) effect of BSA on QD fluorescence at 293 K; (C) Stern–Volmer plots for the fluorescence quenching of QN/QD with the addition of BSA. Conditions: [BSA] = 2.0×10^{-6} mol l^{-1}; [Q] (a–m), 0–4.8×10^{-5} mol l^{-1} at increment of 0.4×10^{-6} mol l^{-1}.

where K_α is analogous to the associative binding constants at the corresponding temperature and R is the gas constant (8.314 J mol^{-1} K^{-1}). Moreover, K_α values were obtained from the emission quenching at the corresponding temperature T, and the values of $\ln K_a$ and $1/T$ with approximate treatment were substituted into the van't Hoff equation. To elucidate the interaction between QN/QD and BSA, the thermodynamic parameters were calculated from the van't Hoff plots. The Gibbs free energy change (ΔG) at different temperatures was then estimated from the following relationship:

$$\Delta G = \Delta H - T\Delta S = -RT \ln K \quad (5)$$

As shown in Fig. S3 and Table 1, ΔG was negative for both cinchona alkaloid isomers and this negative value indicated the spontaneity of the binding interactions between QN/QD with BSA. ΔH and ΔS were found to be −17.54 kJ mol^{-1} and 16.07 J mol^{-1} K^{-1}, −18.88 kJ mol^{-1} and 7.09 J mol^{-1} K^{-1} for the interactions of QN–BSA and QD–BSA, respectively. The negative ΔH and positive ΔS meant that the QN/QD–BSA quenching process was both entropy and enthalpy driven and electrostatic forces played a major role in the ligand–protein complexation. BSA, with an isoelectric point of 5.8, is negatively charged in a PBS buffer of pH 7.4. However, QN/QD is positively charged under the same experimental conditions. Therefore, the electrostatic force between the cationized cinchona alkaloid and the negatively charged BSA facilitates the binding of QN/QD with BSA under physiological pH. The entropy change of the QN–BSA system was larger than that of QD, suggesting the higher binding affinity for QN towards BSA. The difference in the thermodynamic process indicated the different binding behaviors and bound environments of the stereoisomers on the protein.

3.4. Absorption spectra study of the stereoselective interaction

The UV–Vis absorption spectra of BSA influenced by different cinchona alkaloid drugs are shown in Fig. 4S. The result shows that there are two bands in BSA absorbance spectra located at 205 nm and 278 nm, respectively. The absorption of BSA at around 205 nm attributes to the $\pi \rightarrow \pi^*$ transition of characteristic polypeptide C=O backbone structure and the weak peak at 278 nm results from the adsorption of the amino acid residues, such as tyrosine (Tyr), tryptophan (Trp) and phenylalanine (Phe) (Chi, Liu, & Zhang, 2010). With the increasing concentrations of cinchona alkaloid drugs to BSA solution, the intensity of the peak at 205 nm increased and red shifted, suggesting that the formation of QN/QD–BSA complex increased the hydrophobicity of the microenvironment of the aromatic amino acid residues. Meanwhile, the absorbance changes at around 278 nm indicated that cinchona alkaloids could cause slight microenvironmental changes of Trp, which was consistent with the conclusion of fluorescence measurements. When QN/QD was added into protein solution, the BSA molecule denatured and the main chain became loose, resulting in a higher possibility to encounter H_2O, especially for the amide moieties. The bathochromic shift of BSA after the ligand–protein complexation was probably caused by the energy level changes of the π^* electron cloud of H_2O (Shu, Liu, Chen, Chen, & Wang, 2011). In addition, QN and QD had a characteristic peak at around 331 nm. As proteins do not have significant absorbance beyond 300 nm, no absorption of BSA alone in this range (300–360 nm) could be observed. Upon binding with BSA, the shape and intensity of both drugs' absorption bands changed. A reasonable explanation for the absorbance changes at around 331 nm might come from the complex formation between BSA and cinchona alkaloid drugs. The change in the absorbance at 331 nm is indicative of the influence of QN/QD on the BSA spectrum rather than a simple spectral overlap. In addition, as a consequence of the ground-state complex formation, static quenching will result in the perturbation of the absorption spectrum of the fluorophore, while dynamic quenching, caused by collision, will not. The alterations in these absorption peaks also confirmed that the fluorescence quenching mechanisms were mainly static.

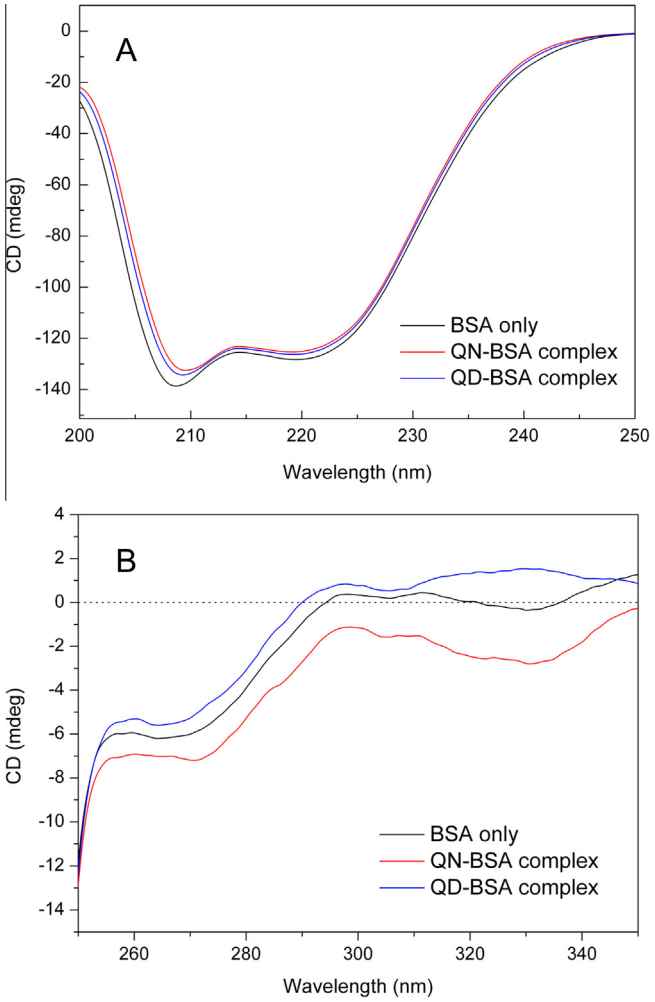

Fig. 4. Circular dichroism spectra of bovine serum albumin in the absence and presence of QN/QD in phosphate buffered saline solution (pH = 7.4) at 298 K. Condition: [BSA] = [Q] = 1.0×10^{-5} mol l^{-1}.

3.5. Circular dichroism analysis

CD spectroscopy is well suitable to monitor the signal associated with the formation of a ligand–protein complex, yielding direct information on the binding interaction and the stereochemistry of the chiral stereoisomers towards proteins (Monti et al., 2009). In order to get further information about the QN/QD–BSA binding mechanism regarding the secondary and tertiary structural changes of the protein, the far and near ultraviolet CD measurements were recorded. As shown in Fig. 4, the far-UV CD spectra of BSA exhibited a typical shape of an α-helix structure (two negative bands at approximately 209 and 222 nm). A reasonable explanation is that the negative peaks at 208–209 nm and 222–223 nm are both from the $n \rightarrow \pi^*$ transfer for the peptide bond of α-helixes. If the CD result was expressed in terms of mean residue ellipticity (MRE) in deg/cm^2/$dmol^{-1}$, the following equation would be used (Eq. (6)):

$$\mathrm{MRE} = \frac{\text{Observed CD}(m\,\text{deg})}{c_p n l \times 10} \tag{6}$$

where c_p is the molar concentration of the protein, n is the number of amino acid residues (583), and l is the path length (1 cm). The α-helical contents were calculated from the *MRE* values at 222 nm using the following equation (Eq. (7)) described in the previous literature:

$$a-\text{helix}\,(\%) = \frac{[\theta]_{222} + 2340}{-30300} \tag{7}$$

where $[\theta]_{222}$ is the observed *MRE* value at 222 nm, 2340 is the MRE of the β-form and random coil conformation cross at 222 nm, and 30300 is the MRE value of a pure α-helix at 222 nm. With the addition of cinchona alkaloid, the intensities of the negative bands at 209 and 222 nm of the protein decreased gradually. The reason maybe that the extended polypeptide structures of BSA caused by the binding of QN/QD led to the exposure of the hydrophobic cavities and perturbation of the microstructures around the aromatic amino acid residues. Additionally, the α-helix content of BSA increased with the additions of drugs when the molar ratio of drug/BSA was 1:1 and the changes induced by the compounds follow the order: QN > QD, which was in accordance with the results of the UV–Vis spectra and fluorescence spectra. From Eqs. (6) and (7), the quantitative analysis results of the α-helix content were obtained. A reduction of the α-helix from 65.17% (free BSA) to 62.89% (QN–BSA 1:1 complex) and 63.67% (QD–BSA 1:1 complex) was observed, indicating the loss of α-helix upon the interaction.

The results show that the influence of QN on the protein conformational change seems to be more prominent than that of QD, which makes BSA unfold and adapt a more incompact conformational state. The different effects of these compounds on the α-helix content of BSA may be associated with the configuration-dependent binding affinities and spatial stereoselectivity of the isomers towards BSA, which further confirms that the interaction between QN/QD and BSA can be influenced by chiral effects involved in the isomer–protein interaction. The QN/QD–BSA complexation could alter the polypeptide structures of BSA, which would then produce the favorable spatial cavities for the binding of BSA with cinchona alkaloid isomers. Besides, the CD spectra of BSA in the presence and absence of the isomers were observed to be similar in shape, thereby indicating that the structure of BSA is predominantly α-helix even after binding.

Moreover, the near UV CD spectrum of BSA showed two minima around 265 and 290 nm (Fig. 4B), characteristic of the disulfide and aromatic chromophores, and reflected the tertiary conformation of the protein (Hossain, Khan, & Kumar, 2011). Upon interaction, the ellipticity value of BSA both enhanced upon binding with QN and QD with the same 1:1 stoichiometry, but reversed in sign of the observed CD bands for QN–BSA system and QD–BSA system. The tertiary structural perturbation of BSA was observed to be different with these two stereoisomers, which were perfectly accounted for by the formation of 1:1 stereoselective ligand–protein complexes with different optical asymmetry.

3.6. Synchronous fluorescence analysis and computational modeling

As mentioned above, QN and QD exhibit different effects on the conformational change of BSA when binding to it, and these conformational changes should be significant in speculating the stereoselective binding properties. Moreover, in synchronous fluorescence spectroscopy, the position shift of the maximum emission wavelength reflects the alterations of polarities around the chromophore molecules. The characteristic information of the tryptophan and tyrosine residues can be obtained when the wavelength intervals ($\Delta\lambda$) between the excitation and emission wavelength are stabilized at 15 or 60 nm, respectively.

The synchronous fluorescence spectra of BSA with various amounts of cinchona alkaloids in Fig. 5 showed that the synchronous fluorescence intensity of BSA decreased regularly with the addition of QN/QD. It was apparent from Fig. 5B that the emission maximum of tryptophan residues showed an obvious red shift

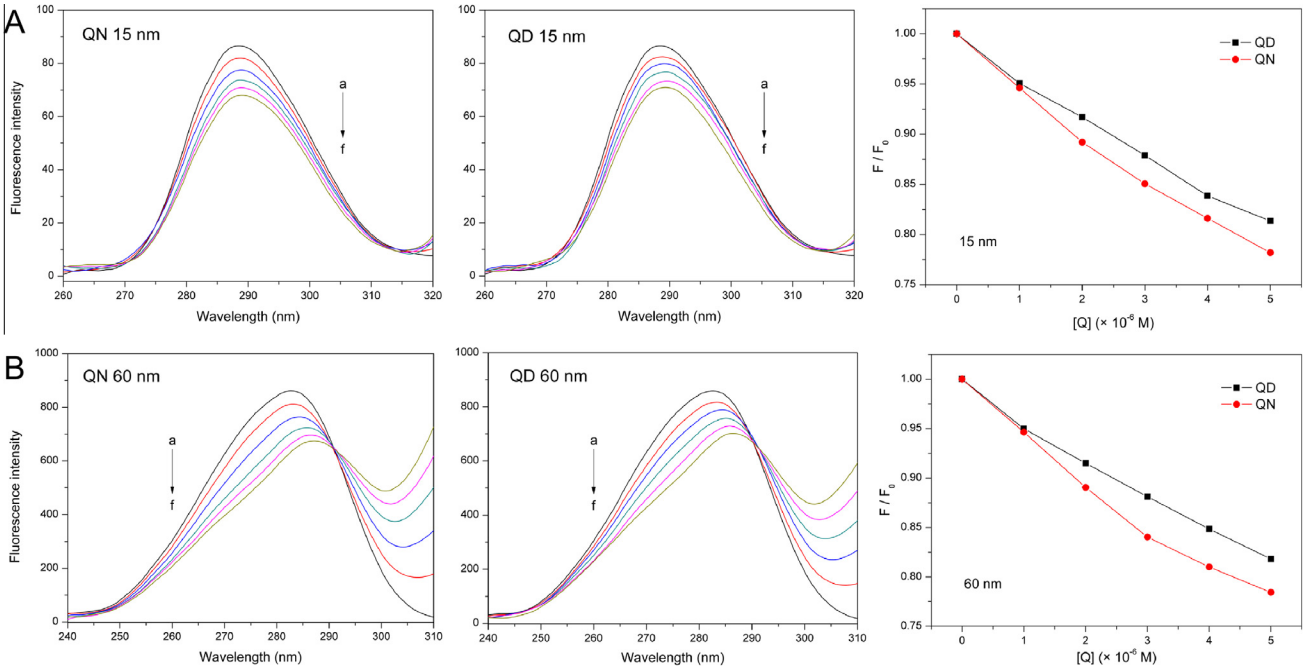

Fig. 5. (A and B) Synchronous fluorescence spectra of BSA: (A) $\Delta\lambda$ = 15 nm, (B) $\Delta\lambda$ = 60 nm and the quenching of BSA synchronous fluorescence by QN/QD. Conditions: [BSA] = 2.0×10^{-6} mol l^{-1}; [Q](a–g), 0–2.5×10^{-5} mol l^{-1} at increment of 0.5×10^{-5} mol l^{-1}; T = 293 K.

(from 283 to 287, 286 nm for QN and QD, respectively), which indicated that the conformation of BSA was changed such that the polarity around the tryptophan residues increased and the hydrophobicity decreased. It was clearly evident that the slope of the QN–BSA system was higher than the QD–BSA system in both cases when $\Delta\lambda$ was set at 15 nm and 60 nm intervals, indicating that QN is situated closer to Tyr and Trp residues compared to QD during the binding interaction. Additionally, it was obvious that a slightly increased quenching was recorded when a $\Delta\lambda$ value of 60 nm was adopted instead of 15 nm. The result suggested that the QN/QD was situated closer to the Trp residue than to the Tyr residue during the ligand–protein complexation process.

Furthermore, we employed the molecular docking method to find the binding site of cinchona alkaloid isomers. The crystal structure of BSA was taken from the Protein Data Bank (entry PDB code 3V03). The docking in Fig. S5 exhibited the most likely binding site of QN/QD on BSA. Almost all of the interactions of QN/QD with BSA were in the vicinity of the active site presented within the 4 Å region that consists of several residues, such as Arg 144, His 145, Arg 196, Ser 428 and Arg 458 for QN–BSA complex, and Glu 186, Leu 189, Ile 455, Arg 435 and Arg 458 for QD–BSA complex. The docking results showed that QN/QD mainly interacted with the positively charged amino acid residues predominately through electrostatic force, and this conclusion was consistent with our conclusion of thermodynamic analysis. It was noteworthy that QN was mainly located at about 11 Å from the Trp, while QD located at about 14 Å from the Trp moiety, which could explain the lower efficiency of QD for the Trp quenching.

4. Conclusion

In summary, the binding to BSA of two cinchona alkaloid isomers, QN and QD, has been systematically studied using FTIR spectroscopy, fluorescence spectroscopy, UV–visible absorption spectroscopy and circular dichroism spectroscopy. Our results highlight the key role of the absolute configuration of stereoisomers–protein system due to the fact that the different stereocenter of chiral compounds can affect its binding mode to BSA. It was found that BSA recognized QN and QD with unequal spectral response, binding affinity and structural perturbation. The FTIR spectra showed that QN and QD interact with both C=O and C–N groups of BSA, resulting in the loss of α-helix structure and the corresponding changes of some other secondary structures with different influence degrees. The fluorescence experimental results indicated that the quenching mechanism of BSA by QN/QD was a static quenching procedure. The electrostatic interactions played a major role during the ligand–protein complexation process. Synchronous fluorescence and molecule docking proved that QD was farther from Trp and Tyr than that of QN, resulting in a much lower efficiency for fluorescence quenching of BSA. The obtained binding constants for QN/QD with BSA were in the intermediate range, the relatively low binding affinities indicated that the binding of QN/QD to BSA might be nonspecific. The binding affinity of QN to BSA was stronger than that of QD due to their different spatial configuration under physiological conditions, leading to the recognition discrepancy of BSA towards QN and QD. The spectroscopic methods applied here proved that the polypeptide backbone and chromophore amino acids of BSA changed and experienced a micro-environmental alteration after ligand–protein complex formation. Besides, the influence on the conformational change of BSA induced by QN was more obvious than that of QD. The studies indicated that the stereoisomers with different chiral center could influence the ligand–protein interactions.

Acknowledgments

The authors gratefully acknowledge the financial support from the National Natural Science Foundation of China (No. 20875055 and 51402294), Natural Science Foundation of Fujian Province, China (No. 2013J01388), State Key Lab of Structural Chemistry, Fujian Institute of Research on the Structure of Matter and Opening Research Foundation of Key Laboratory of Biomedical Material in Tianjin city.

Appendix A. Supplementary data

Supplementary data associated with this article can be found, in the online version, at http://dx.doi.org/10.1016/j.foodchem.2015.02.040.

References

Belatik, A., Hotchandani, S., Carpentier, R., & Tajmir-Riahi, H. A. (2012). Locating the binding sites of Pb(II) ion with human and bovine serum albumins. *PLoS ONE, 7*, e36723.

Callaway, J. L., & Tate, W. E. (1974). Toxic epidermal necrolysis caused by gin and tonic. *Archives of Dermatology, 109*, 909.

Carter, D. C., & Ho, J. X. (1994). Structure of serum-albumin. *Advances in Protein Chemistry, 45*(45), 153–203.

Charbonneau, D. M., & Tajmir-Riahi, H. A. (2010). Study on the interaction of cationic lipids with bovine serum albumin. *Journal of Physical Chemistry B, 114*, 1148–1155.

Chi, Z. X., Liu, R. T., & Zhang, H. (2010). Noncovalent interaction of oxytetracycline with the enzyme trypsin. *Biomacromolecules, 11*, 2454–2459.

Chi, Z. X., & Liu, R. T. (2011). Phenotypic characterization of the binding of tetracycline to human serum albumin. *Biomacromolecules, 12*, 203–209.

Horie, M., Oishi, M., Ishikawa, F., Shindo, T., Yasui, A., Ogino, S., et al. (2006). Liquid chromatographic analysis of *Cinchona alkaloids* in beverages. *Journal of Aoac International, 89*, 1042–1047.

Hossain, M., Khan, A. Y., & Kumar, G. S. (2011). Interaction of the anticancer plant alkaloid sanguinarine with bovine serum albumin. *PLoS ONE, 6*.

Izake, E. L. (2007). Chiral discrimination and enantioselective analysis of drugs: An overview. *Journal of Pharmaceutical Sciences, 96*, 1659–1676.

Karle, J. M., Karle, I. L., Gerena, L., & Milhous, W. K. (1992). Stereochemical evaluation of the relative activities of the cinchona alkaloids against plasmodium-falciparum. *Antimicrobial Agents and Chemotherapy, 36*, 1538–1544.

Kellogg, R. M., Dijkstra, G. D. H., Wynberg, H., Svendsen, J. S., Marko, I., & Sharpless, K. B. (1989). Conformational study of cinchona alkaloids – A combined Nmr, molecular mechanics, and X-ray approach. *Journal of the American Chemical Society, 111*, 8069–8076.

Kuhnemuth, R., & Seidel, C. A. M. (2001). Principles of single molecule multiparameter fluorescence spectroscopy. *Single Molecules, 2*, 251–254.

Kumar, C. V., Buranaprapuk, A., & Sze, H. C. (2001). Large chiral discrimination of a molecular probe by bovine serum albumin. *Chemical Communications*, 297–298.

Lakowicz, J. R. (1999). *Principles of fluorescence spectroscopy* (2nd ed.). New York: Kluwer Academic/Plenum.

Lakowicz, J. R. (2006). *Principles of fluorescence spectroscopy* (third ed.). New York: Springer.

Lanone, S., Andujar, P., Kermanizadeh, A., & Boczkowski, J. (2013). Determinants of carbon nanotube toxicity. *Advanced Drug Delivery Reviews, 65*, 2063–2069.

Lazaro, E., Lowe, P. J., Briand, X., & Faller, B. (2008). New approach to measure protein binding based on a parallel artificial membrane assay and human serum albumin. *Journal of Medicinal Chemistry, 51*, 2009–2017.

Liu, Y., Chen, M. M., Luo, Z. P., Lin, J. J., & Song, L. (2013). Investigation on the site-selective binding of bovine serum albumin by erlotinib hydrochloride. *Journal of Biomolecular Structure & Dynamics, 31*, 1160–1174.

Lu, H. (2007). Stereoselectivity in drug metabolism. *Expert Opinion on Drug Metabolism & Toxicology, 3*, 149–158.

Mantsch, H. H., & Chapman, D. (1996). *Infrared spectroscopy of biomolecules*. New York: Wiley-Liss.

Martin, V. I., Rodriguez, A., Maestre, A., & Moya, M. L. (2013). Binding of cationic single-chain and dimeric surfactants to bovine serum albumin. *Langmuir, 29*, 7629–7641.

Monti, S., Ottani, S., Manoli, F., Manet, I., Scagnolari, F., Zambelli, B., et al. (2009). Chiral recognition of 2-(3-benzoylphenyl)propionic acid (ketoprofen) by serum albumin: an investigation with microcalorimetry, circular dichroism and molecular modelling. *Physical Chemistry Chemical Physics, 11*, 9104–9113.

Ohira, A., Yamaguchi, S., Miyagi, T., Yamamoto, Y., Yamada, S., Shiohira, H., et al. (2013). Fixed eruption due to quinine in tonic water: A case report with high-performance liquid chromatography and ultraviolet A analyses. *Journal of Dermatology, 40*, 629–631.

Otagiri, M., & Chuang, V. T. G. (2006). Stereoselective binding of human serum albumin. *Chirality, 18*, 159–166.

Pace, C. N., Shirley, B. A., McNutt, M., & Gajiwala, K. (1996). Forces contributing to the conformational stability of proteins. *FASEB Journal, 10*, 75–83.

Peters, T. (1985). Serum-albumin. *Advances in Protein Chemistry, 37*, 161–245.

Ross, P. D., & Subramanian, S. (1981). Thermodynamics of protein association reactions – forces contributing to stability. *Biochemistry, 20*, 3096–3102.

Shu, Y., Liu, M. L., Chen, S., Chen, X. W., & Wang, J. H. (2011). New insight into molecular interactions of imidazolium ionic liquids with bovine serum albumin. *Journal of Physical Chemistry B, 115*, 12306–12314.

Vaden, T. D., de Boer, T. S., MacLeod, N. A., Marzluff, E. M., Simons, J. P., & Snoek, L. C. (2007). Infrared spectroscopy and structure of photochemically protonated biomolecules in the gas phase: A noradrenaline analogue, lysine and alanyl alanine. *Physical Chemistry Chemical Physics, 9*, 2549–2555.

Vaughan, W. M., & Weber, G. (1970). Oxygen quenching of pyrenebutyric acid fluorescence in water. A dynamic probe of the microenvironment. *Biochemistry, 9*, 464–473.

Worden, A. N., Frape, D. L., & Shephard, N. W. (1987). Consumption of quinine hydrochloride in tonic water. *Lancet, 1*, 271–272.

Zaugg, S., & Thormann, W. (2001). Capillary electrophoretic separation, immunochemical recognition and analysis of the diastereomers quinine and quinidine and two quinidine metabolites in body fluids. *Journal of Pharmaceutical and Biomedical Analysis, 24*, 785–799.

Zhang, G. W., & Ma, Y. D. (2013). Mechanistic and conformational studies on the interaction of food dye amaranth with human serum albumin by multispectroscopic methods. *Food Chemistry, 136*, 442–449.

Zhao, X. C., & Liu, R. T. (2012). Recent progress and perspectives on the toxicity of carbon nanotubes at organism, organ, cell, and biomacromolecule levels. *Environment International, 40*, 244–255.